Numerical Simulation of Low-Reynolds-Number and High-Lift Airfoil S1223

Rong Ma, Peiqing Liu

***Abstract* — The range of Reynolds number under studied by airfoil aerodynamics problem for the application of the propeller of low-dynamic aircrafts in Near Space is between 10^5 to 10^6, which belongs to the scope of low Reynolds number. But in the low Reynolds number condition, the aerodynamic characteristics of airfoil show some new properties, such as the rapidly descending maximum lift-to-drag ratio of common airfoils and the non-linear phenomena of the symmetrical airfoils in the small angle of attack especially near 0°, etc. Thus it is necessary to do some relative research on the numerical simulation of low-Reynolds-number and high-lift airfoils. Generally, the aerodynamic performance of airfoil for the application of the propeller of low-dynamic aircrafts in Near Space is mainly effected by Reynolds number, Mach number, the angle of attack , the airfoil chord length b and the airfoil relative thickness $\overline{C} = \frac{C}{b}$, namely f (Re, Ma, α , b, $\overline{C}$). Due to the low speed and small Mach number, the aerodynamic performance of airfoils can ignore the effect of Mach number. Airfoil S1223 which has a good aerodynamic performance in the low Reynolds number condition was focused and chosen finally for the numerical simulation of low-Reynolds-number and high-lift airfoils using FLUENT computational software. The numerical simulation is using the Spalart-Allmaras turbulence model and is considering the treatment method of surface flow near wall in the condition of low free stream velocity V_0 =20m/s through the transformation of the following three pneumatic parameters including Reynolds number, the angle of attack α and the airfoil relative thickness $\overline{C} = \frac{C}{b}$. Finally, the aerodynamic performance of the numerical simulation for airfoil S1223 is shown in the pictures of the lift curve, the drag curve, the moment of force curve, streamline diagram and the pressure distribution contour diagram around the surface. In order to verify the rationality of the numerical simulation, the aerodynamic performance data of the numerical simulation are compared with the experimental data of airfoil S1223 with the relative thickness of 12.13%, which prove the numerical simulation of low-Reynolds-number and high-lift airfoil S1223 is reasonable.**

***Index Terms*: High Lift Airfoil, Low Reynolds Number, Numerical Simulation, Airfoil S1223.**

I. Introduction

Along with the developments of high technology in aeronautics, astronautics and materials, and the surge in oil prices caused by the World Wide Oil Crisis from the 1960s, it is more and more prosperous in the aircraft family members from hot balloon to the space station, and from all types of battle planes and Micro Air Vehicles to spacecrafts. But recently, there has been the emergence of a new star for the Air Combat in this big family that is the low-dynamic vehicle in Near Space.

The altitude of Near Space is about 20km to 100km apart from the ground, which is between the highest flight altitude of plane and the minimum orbit height of satellite. When the low-dynamic vehicle flies in the Near Space, it shows the advantages of long endurance and the functions of huge transport aircraft, so it is widely used in the place of antisubmarine scout and information platform of the army, see Fig.1. By the lately design of the advanced low dynamic vehicles in Near Space, such as heavy-duty airship Walrus, antimissile airship HAA and some high-altitude long-endurance unmanned airplanes including Tier, Helios Pathfinder, etc, the propulsion system is the general high-power DC motor-driven propeller system, see Fig.2.

Fig.1 high altitude information platform

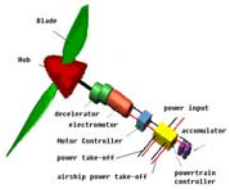

Fig.2 propeller system composition

But the great differences of aerodynamic parameters in the high altitude, such as the smaller atmospheric density, the lower air pressure, the bigger air kinematic viscosity coefficient compared with aerodynamic parameters of the low altitude, make the range of Reynolds number under studied by airfoil aerodynamics problem is between 10^5 to 10^6, which belongs to the scope of low Reynolds number. But in the low Reynolds number condition, the aerodynamic characteristics of airfoil shows some new characteristics, such as the rapidly descending maximum lift-to-drag ratio of common airfoils[1] and the non-linear phenomena of the symmetrical airfoils in the small angle of attack especially near 0° present the non-linear phenomena[2][3], etc.

A lot of researches show that the above phenomena under the low Reynolds number condition are closely related with the laminar flow separation phenomenon[4]. It is well known that the determination of the boundary separating point is always a great obstacle for the airfoil design which has been estimated by the experience and the experiments. So it always needs a long period, a high cost and a rich experience. But fortunately, with the emergence of the high-speed electronic computers, numerical simulation technology is applied to airfoil design more frequently.

Computational Fluid Dynamics (CFD) is one effective method of studying fluid dynamics, which could describe the complex flow of geometric boundary, evaluate the

Rong Ma, candidate Ph.D, is with the Beijing University of Aeronautics and Astronautics, Beijing, 100191 China. She is now as visiting student in the Cranfield University, Bedfordshire MK43 0AL, United Kingdom (Phone: (+44)758-886-8994 or 755-196-5744; E-mail: r.ma@cranfield.ac.uk).

Peiqing Liu, Professor, with the Beijing University of Aeronautics and Astronautics, Beijing, 100191 China (E-mail: lpq@buaa.edu.cn).

preliminary airfoil design rapidly and make prompt changes. So it can greatly reduce the cost, time and the risks of repeated experiments which become a kind of important design and calculation method and is used in the airfoil design and the flow field analysis more frequently in recent years.

II. Aerodynamic Characteristics of Propeller Airfoil at High Altitude

The cruising altitude scope of low dynamic vehicles in Near Space is generally between 20km and 100km where is low air-density, almost constant air-temperature, the horizontal-direction movement and no thunderstorm on climate change.

A. Low Reynolds Number Effect

Atmospheric density decreases with the increase of height. For example, the air density is 0.08803kg/m^3 at the height of 20km, while it is 1.225kg/m^3 at sea level. At the same time, the air kinematic viscosity coefficient increases with the increase of height. For example, the air kinematic viscosity coefficient is 16.1x10^{-5}m^2/s at the height of 20km, while it is 1.46x10^{-5}m^2/s at the sea level. Therefore, the range of Reynolds number under studied by airfoil aerodynamics problem for the application of the propeller of low-dynamic aircrafts in Near Space is between 10^5 to 10^6, which belongs to the scope of low Reynolds number. But in the low Reynolds number condition, the aerodynamic characteristics of airfoil shows some new characteristics. Firstly, there is the appearance of laminar flow separation bubble even in small attack angles (see Fig.3), which brings the slowly increased lift coefficient and the rapidly increased drag coefficient. Along with the increase of attack angle, lift coefficient event does not change anymore but the drag coefficient still increases rapidly which makes the airfoil maximum lift-to-drag ratio drops rapidly.

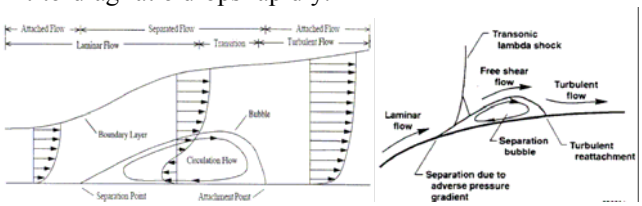

a) Airfoil boundary layer in low Mach b) Airfoil boundary layer in high Mach

Fig.3 boundary layer schematic diagram on the upper surface of low Reynolds number airfoil

Then, the non-linear phenomena of the symmetrical airfoils in the small angle of attack especially near 0^o present the non-linear phenomena. Judging from the above, the efficiency of propeller decreases sharply and aerodynamic performance of propeller reduces dramatically.

B. The High Mach Number Effect on Blade-tip Airfoil Profile

The sound velocity decreases with the increase of altitude. For example, the air sound velocity is 295.07m/s at the height of 20km, while it is 340.3m/s at the sea level. So at a high altitude, the Mach number of blade-tip airfoil profile is larger than the one at the sea level and the shock effect increases at the same time, see Fig.3 (b). Thereby, the aerodynamic performance of airfoil and propeller is significantly reduced.

III. Airfoil Selection

The airfoil S1223 was chosen over other low-Reynolds-number airfoils with known good performance at low Reynolds numbers for the constant section propeller which are shown in Table 1.

Table1 Tabulated data for Low Reynolds Number airfoils [6][7]

Airfoil	$C_{L\max}$	$C_{m,c/4}$	Re	Reference
E214	1.25	-0.11	2 x 10^5	27
E423	2.00	-0.25	2 x 10^5	20
FX 63-137	1.75	-0.17	2 x 10^5	Present Paper
M06-13-128	1.52	0.00	2 x 10^5	Present Paper
LA2573A	1.86	0.02	2.5 x 10^5	9
LNV109A	1.87	-0.02	2.5 x 10^5	9
S1223	2.23	-0.29	2 x 10^5	Present Paper
S3021	1.17	-0.07	2 x 10^5	27

Based on predictions [6][7]

The contour of airfoil S1223 is shown in Fig.4. Experimental results were found for airfoil S1223 that had been tested in the University of Illinois at Urbana-Champaign (UIUC) subsonic wind tunnel[5]. Lift characteristics for a Reynolds number of are shown in Fig.5 and polar curve for airfoil S1223 is shown in Fig.6. The results indicate that the maximum lift coefficient is approximately 2.2, which clearly validates the aforementioned design philosophy. This characteristic is important for some UAVs that operate with the airfoil near to achieve low-speed flight requirements for loiter, cruise, or landing. Therefore, the low-Reynolds-number and high-lift airfoil S1223 is the final choice for the numerical simulation and the preliminary evaluation of aerodynamic performance.

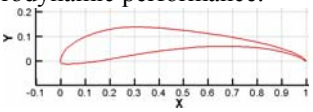

Fig.4 Contour of airfoil S1223

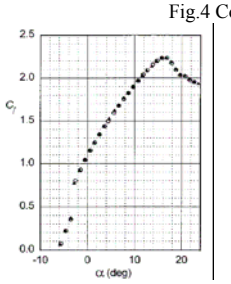

Fig.5 Lift characteristics for airfoil S1223 at Re=2x10^5

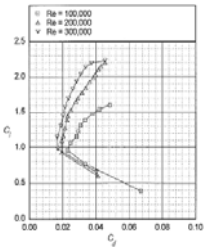

Fig.6 polar curve for airfoil S1223

IV. Turbulence Model

A. Spalart-Allmaras Model in FLUENT

FLUENT software could provide many turbulence models including Spalart-Allmaras model, k-model and the Reynolds stress model and large eddy simulation, etc. Spalart-Allmaras turbulence model was put forward by S. Allmaras in 1992, which is a simple-equation turbulence model through solving the turbulence viscosity of the transport equations. It is not deduced from the simplification of k-ε equation as other single-equation turbulence models, but from the experience and the dimensional analysis. Nowadays, Spalart-Allmaras turbulence model has been improved and developed into a single-equation turbulence model applied to the turbulent flow along the solid wall boundary including the laminar flow, which has a smaller calculation, a better stability and a higher precision compared with the two-equation turbulence

model.

In addition, Spalart-Allmaras turbulence model is a local-type model, which don't have any non-local item in the its equation like y^+ ($y^+ = \frac{y}{\mu}\sqrt{\rho\tau_w}$), etc. So it doesn't need any special treatment in a complex flowfield with many physical surfaces and could be used more conveniently.

Lately, Spalart-Allmaras turbulence model is very popular and mainly used for analysis and calculation of aerodynamic performance to resolve aerodynamic problems with boundary constraint in aeronautics and astronautics research field, especially for the problem with reverse pressure gradient in the boundary layer. The aerodynamic calculation results of Spalart-Allmaras turbulence model prove very effective, so it is widely recognized in the airfoil and the wing fields.

In view of the above consideration, the numerical simulation of low-Reynolds-number and high-lift airfoil S1223 chooses the Spalart-Allmaras turbulence model as the first selection.

B. *Wall Condition*

In the wall surface, when the value of turbulent kinematic viscosity coefficient is set to 0, the shear stress of the wall is resolved by the relationship of stress-strain with laminar flow, which is shown in (1).

$$\frac{u}{u_\tau} = \frac{\rho u_\tau y}{\mu} \tag{1}$$

If the grid is rough enough to be used to solve laminar bottom, then it is supposed that the grid centroid should be located in the logarithmic region of boundary layer. So according to the wall area principle, the shear stress of the wall is resolved, which is shown in (2).

$$\frac{u}{u_\tau} = \frac{1}{k}\ln E\left(\frac{\rho u_\tau y}{\mu}\right) \tag{2}$$
$$k = 0.419, E = 9.793$$

V. The Numerical Simulation Method

A. *The Grid Generation*

The numerical simulation of low-Reynolds-number and high-lift airfoils S1223 is using Gridgen software to build the calculated model whose chord length is 1, using elliptic method to generate C type grid. The minimum distance in normal direction of the first layer of the grid from the ground is $10^{-5,}$ and the far field boundary is 20 times as long as chord length. The total grid nodes are 122196, see Fig.7.

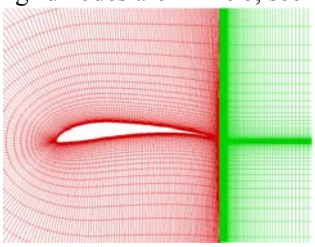

Fig.7 Calculation field and computational grid of airfoil S1223

Grid is generated by using elliptic equation method whose spacing rate is adjusted through controlling the source term. To improve the orthogonality of grid near wall, the algebraic method is used to smooth the surface grid. In the numerical calculation, Reynolds number of the free stream is 1.25×10^5 and Mach number of the free stream is about 0.1 consumed with local time step. The entrance boundary is given by using the free stream, while the export boundary conditions is using Riemann reflectionless boundary. The wall surface is taking no-sliding condition, and the initial condition of the flowfield is setting in accordance with the free stream.

B. *The Flowfield Calculation*

The calculation of flowfiled chooses the implicit solver based on pressure and the Spalart-Allmaras turbulence model of FLUENT computational software. The pressure-speed coupled method adopts SIMPLEC algorithm and the calculation accuracy is 10^{-4}.

VI. Reliability Analysis of Fluent Aerodynamic Calculated Results

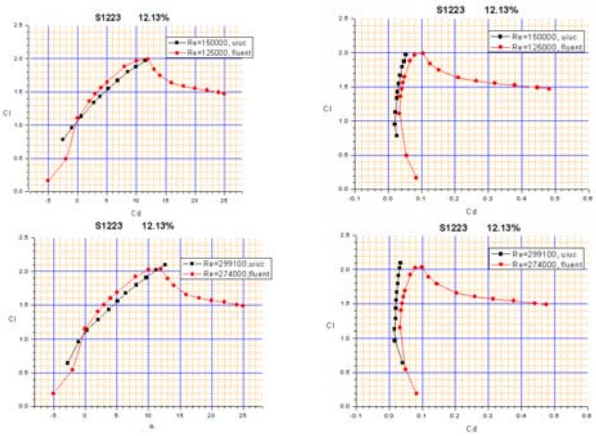

Fig.8 Comparison between numerical simulation data and experiment data of airfoil S1223 with relative thickness of 12.13%

From Fig.8, it can be clearly seen that the numerical simulation results of airfoil S1223 with relative thickness of 12.13% in the condition of Re=125000 and Re=274000 are almost identical with the corresponding experimental, which can be fully confirmed that the numerical simulation of the low-Reynolds-number and high-lift airfoil is reasonable.

VII. The Work Plan for the Numerical Simulation Calculation

The numerical simulation target is mainly on low-Reynolds-number and high-lift airfoil S1223 by alternating three aerodynamic parameters including Reynolds number, attack angle α and airfoil relative thickness $\overline{C} = \frac{C}{b}$ (where b is airfoil chord) in the condition of free stream velocity=20m/s. The lift coefficient Cl=f (V_0, Re, Ma, α, $\overline{C}$), drag coefficient Cd=f (V_0, Re, Ma, α, $\overline{C}$)), torque coefficient Cm= f (V_0, Re, Ma, α, $\overline{C}$)) and lift-drag ratio Cl/Cd=f (V0, Re, Ma, α, $\overline{C}$) of airfoil S1223 are calculated separately.

Seven different relative thicknesses are calculated as the following.

$\overline{C} = \frac{C}{b}$ = 5%, 10%, 11.93%, 12.13%, 15%, 20%, 25%

Eighteen different attack angles are calculated as the following.

α = -5, -2, 0, 2, 3, 4, 5, 8, 10, 12, 13, 14, 16, 18, 20, 22, 24, 25.

Five different Reynolds numbers are calculated as Table 2.

Table 2 Reynolds Numbers in Different Height

H(km)	Re(×10^5)
20	1.25
15	2.74
10	5.60
8	6.90
5	9.05

VIII. Calculation Results and Analysis

For 18 different attack angles and 5 different Reynolds numbers, the lift curve, drag curve, torque curve and lift-to-drag curve of airfoil S1223 of 7 different relative thicknesses are shown in Fig.9~15 as numerical simulation results.

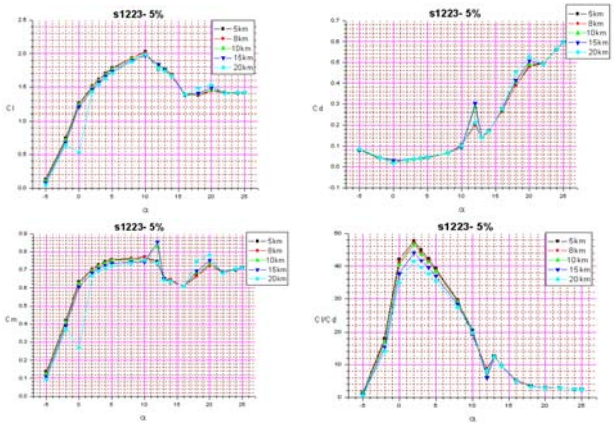

Fig.9 Lift curve, drag curve, torque curve and lift-to-drag curve of airfoil S1223 with the relative thickness of 5%

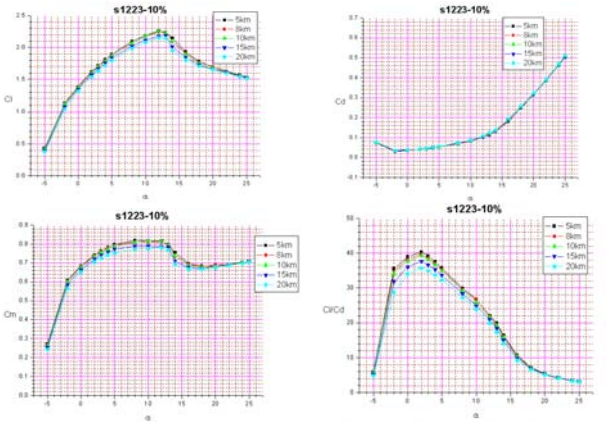

Fig.10 Lift curve, drag curve, torque curve and lift-to-drag curve of airfoil S1223 with the relative thickness of 10%

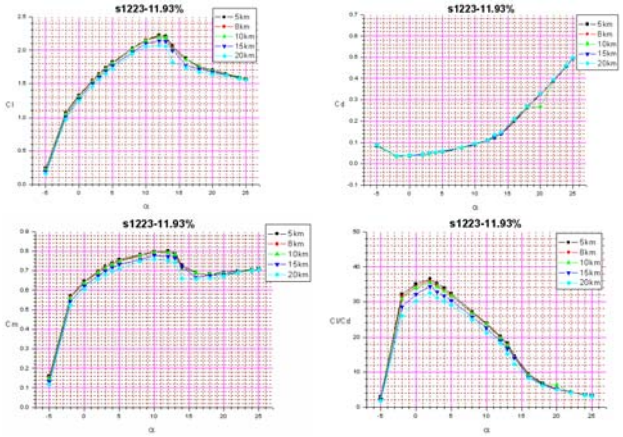

Fig.11 Lift curve, drag curve, torque curve and lift-to-drag curve of airfoil S1223 with the relative thickness of 11.93%

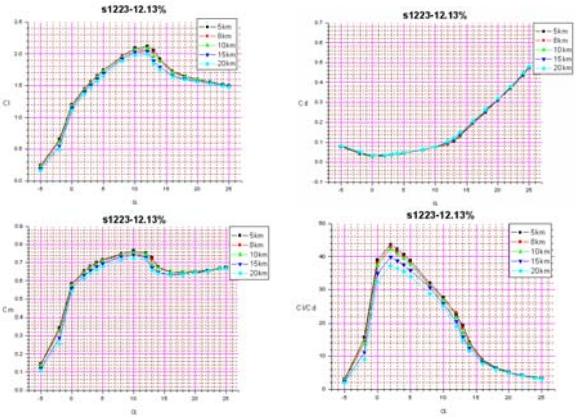

Fig.12 Lift curve, drag curve, torque curve and lift-to-drag curve of airfoil S1223 with the relative thickness of 12.13%

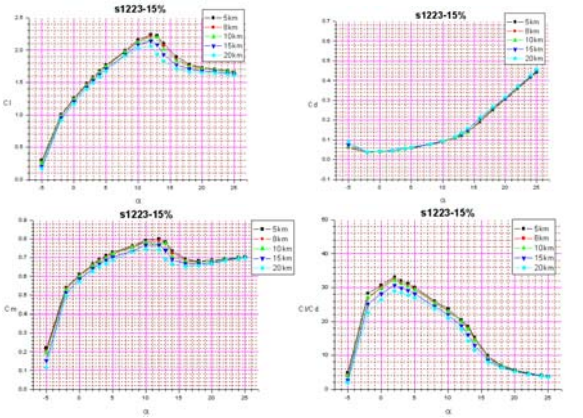

Fig.13 Lift curve, drag curve, torque curve and lift-to-drag curve of airfoil S1223 with the relative thickness of 15%

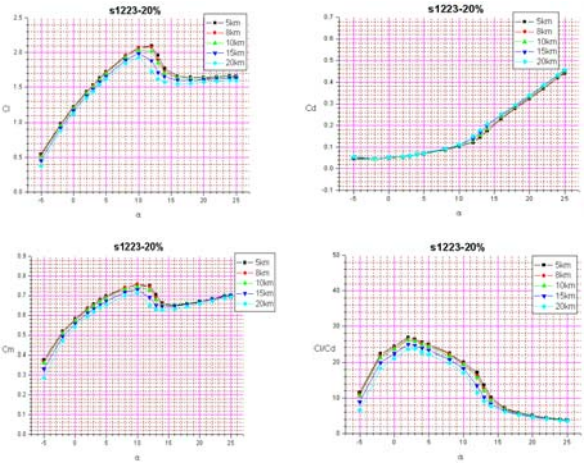

Fig.14 Lift curve, drag curve, torque curve and lift-to-drag curve of airfoil S1223 with the relative thickness of 20%

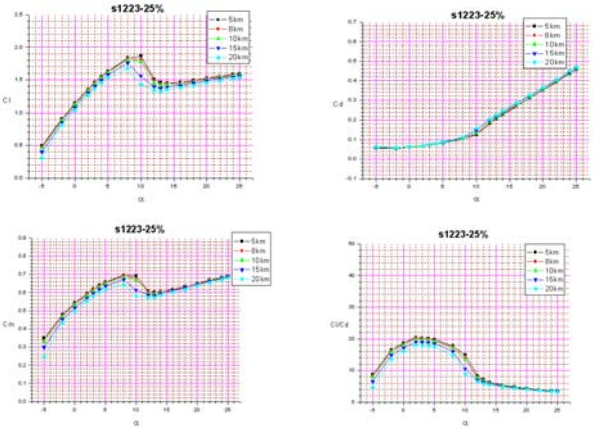

Fig.15 Lift curve, drag curve, torque curve and lift-to-drag curve of airfoil S1223 with the relative thickness of 25%

From the above numerical simulation data diagrams, some conclusions can be obtained as follows:

1) For low-Reynolds-number and high-lift airfoil S1223, the aerodynamic calculation results are influenced by relative thickness, especially the maximum lift-to-drag ratio. The thick airfoil produces low lift-to-drag ratio, thereby reducing the propeller efficiency. At the same time, in the range of attack angle α= -2° ~10° , the lift-to-drag ratio is influenced greatly by the Reynolds number, that is the lift-to-drag ratio decreases with the reduction of Reynolds number.
2) For airfoil S1223 of large relative thicknesses (20% and 25%) and thin relative thickness (5%), stalling attack angle decreases more obviously than any other relative thicknesses. And for airfoil S1223 of large relative thicknesses (20% and 25%), it is the greatest for the stalling attack angle when influenced by the Reynolds number, that is the stalling attack angle decreases with the reduction of Reynolds number.
3) Except for the thin relative thickness (5%), it could be clearly seen that Cl_{max} is affected obviously by the Reynolds number which is decreased with reduction of Reynolds number in the range of attack α=5° ~18° in any other relative thickness of airfoil S1223.

IX. CONCLUSION

Through the comparison and the analysis of overall aerodynamic parameters of airfoil S1223 with various relative thicknesses, it can be seen that aerodynamic parameters (especially lift-to-drag ratio) of low-Reynolds-number and high-lift airfoil S1223 are greatly affected by relative thickness and Reynolds number. Airfoil S1223 with the relative thickness of 12.13% and 5% own the best performance based on the comparison and analysis. So it is suggested that the airfoil S1223 with relative thickness of 5% can be used for the blade tip and the airfoil S1223 with relative thickness of 12.13% can be used for blade root. Moreover, further optimized design research will be carried on based on low-Reynolds-number and high-lift airfoil S1223.

APPENDIX

The streamline diagram and the pressure distribution contour diagram of airfoil S1223 with the relative thickness of 12.13% are shown in Fig.16~23 below under several attacks at height H=20km ($Re=1.25\times10^5$).

A. The Attack Angle $\alpha=-2^o$

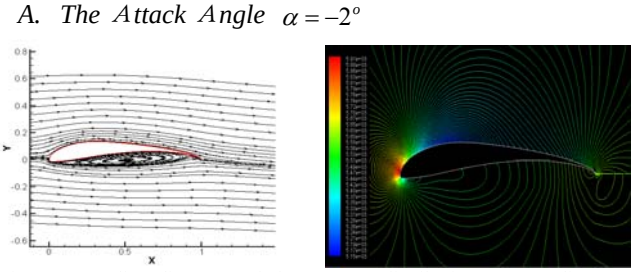

Fig.16 Streamline diagram and the pressure distribution contour diagram of airfoil S1223 with the relative thickness of 12.13% at the attack angle of -2°

Since adverse pressure gradient has a directly proportional relationship with airfoil curvature, the adverse pressure gradient is large under a negative attack angle due to large curvature of lower surface.

As shown in the streamline diagram of α= -2° , in the condition of low Reynolds number and negative attack, it is hard for air flow to overcome the effect of adverse pressure gradient. So the long laminar separation bubble takes place at a lower surface of airfoil which also can be seen from the pressure distribution contour diagram. Started from the leading edge, the pressure changes fast from the red high pressure area to the blue low pressure area at the lower surface of airfoil.

Besides, as shown in the pressure distribution contour diagram, there is no great change for pressure. That is because this separation bubble is closed.

B. The Attack Angle $\alpha=0^o$

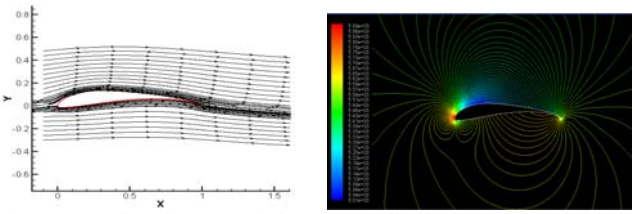

Fig.17 Streamline diagram and the pressure distribution contour diagram of airfoil S1223 with the relative thickness of 12.13% at the attack angle of 0°

As can be seen from Fig.17, airflow attaches the surface of airfoil at the attack angle of 0° .

C. The Attack Angle $\alpha=2^o$

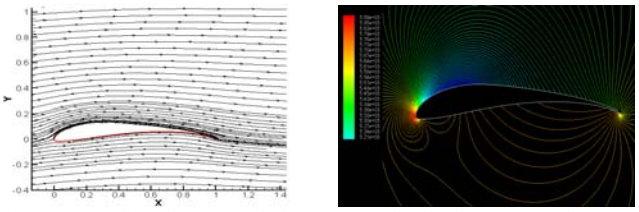

Fig.18 Streamline diagram and the pressure distribution contour diagram of airfoil S1223 with the relative thickness of 12.13% at the attack angle of 2°

As can be seen from Fig.18, there is a little air separation phenomenon at trailing edge at the attack angle of 2° . The reason is that the flow speed is slower and the pressure is higher in the upper surface than the lower surface, so the air flows from the lower surface to the upper surface through the stationary point at the trailing edge.

D. The Attack Angle $\alpha=5^o$

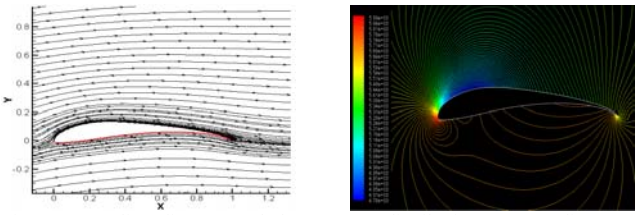

Fig.19 Streamline diagram and the pressure distribution contour diagram of airfoil S1223 with the relative thickness of 12.13% at the attack angle of 5°

As can be seen from Fig.19, the flow separation moves forward slowly at the attack angle of 5° .

E. The Attack Angle $\alpha = 8^o$

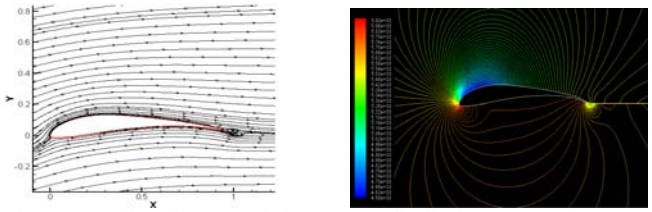

Fig.20 Streamline diagram and the pressure distribution contour diagram of airfoil S1223 with the relative thickness of 12.13% at the attack angle of 8°

As can be seen from Fig.20, two reverse direction vortexes appear at trailing edge at the attack angle of 8° . The previous one is a small-range air separation as a result of the adverse pressure gradient which the upper surface can not overcome. The other one is still a small-range air separation which is caused by the flow from the lower surface to the stationary point of the upper surface.

F. The Attack Angle $\alpha = 10^o$

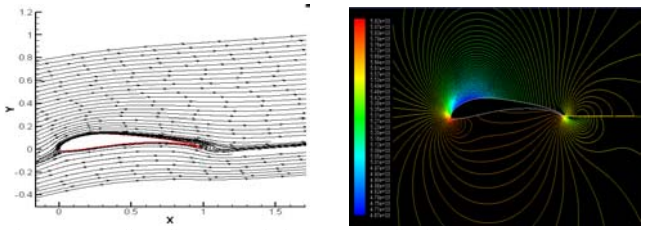

Fig.21 Streamline diagram and the pressure distribution contour diagram of airfoil S1223 with the relative thickness of 12.13% at the attack angle of 10°

As can be seen from Fig.21, the two small separation bubbles on the upper and lower surfaces separately form a clockwise flow separation at the attack angle of 10° .

G. The Attack Angle $\alpha = 12^o$

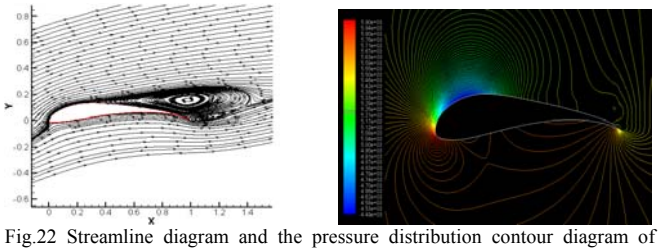

Fig.22 Streamline diagram and the pressure distribution contour diagram of airfoil S1223 with the relative thickness of 12.13% at the attack angle of 12°

From the formed closed circle vortex in the streamline diagram and the closed contour in the pressure distribution contour diagram, it can be seen clearly that the flow has been separated completely at the attack angle of 12° . Thus stalling angle of attack is proved to be up to 12° , according to the previous airfoil aerodynamic data.

ACKNOWLEDGMENT

Rong Ma thanks Prof. Peiqing Liu for his constant guidance as my supervisor, and then thanks to Dr. Qiulin Qu for his sincere instruction and help, and finally thanks to my husband Mr. Xingxiao Liang and my parents for their encouragement and support.

REFERENCES

[1] MUELLER T. J., "The Influence of Laminar Separation and Transition on Low Reynolds Number Airfoil Hysteresis (Translation Journals style)" , Journal of Aircraft, vol.22, 1985, pp. 764-770.
[2] Michael S. Selig, James J. Guglielmo, Andy P. Broeren, "Experiments on Airfoils at Low Reynolds Number (Translation Journals style)", AIAA-1996-62, 34th Aerospace Sciences Meeting and Exhibit, NV, Jan.1996, pp. 15-18.
[3] Peng Bai, Erjie Cui, Feng li, Weijiang Zhou, "Symmetrical airfoil low Reynolds number of small attack angle lift coefficients nonlinear phenomena research (Journals style)", Chinese Journal of Theoretical and Applied Mechanics, vol.38, 2006, pp. 1-8.
[4] Ziqiang Zhu, Xiaolu Wang, Zongcheng Wu, "Aerodynamic Characteristics of Small/Micro Unmanned Aerial Vehicles and Their Shape Design (Journals style)", ACTA Aeronautica ET Astronautica Sinica, vol.27, 2006, pp. 353-364.
[5] Michael S. Selig and James J. Guglielmo, "High-Lift Low Reynolds Number Airfoil Design (Translation Journals style)", Journal of aircraft, vol. 34, No. 1, Jan. 1997.
[6] Selig, M. S., Guglielmo, J. J., Broeren, A. P., and Gigue´re, P., "Summary of Low-Speed Airfoil Data (Translation Journals style)", vol. 1, SoarTech Publications, Virginia Beach, VA, 1995.
[7] Selig, M. S., and Guglielmo, J. J., "High-Lift Low Reynolds Number Airfoil Design", AIAA Paper 94-1866, June 1994.
[8] Shunzhao Zhang, Guixiang Cui, Chunxiao Xu, Theory and Modeling of Turbulence (Book style), Tsinghua University Press, CN: Beijing, 2005.
[9] L. Danielle Koch, "Design and Performance Calculations of a Propeller for Very High Altitude Flight", NASA/TM, 1998-206637.
[10] Wael A. Mokhtar, "A Numerical Parametric Study of High-Lift Low Reynolds Number Airfoils", AIAA 2005-1355
[11] Miley, S. J., "On the Design of Airfoils for Low Reynolds Numbers", proceedings of the AIAA/MIT/SSA 2nd International Symposium of the Technology and Science of Low-Speed and Motorless Flight, Soaring Society of America, Los Angeles, CA, 1974, pp.82 - 96 (AIAA Paper 74-1017, Sept. 1974).
[12] Eppler, R., Airfoil Design and Data (Book style), Springer-Verlag, New York, 1990.
[13] Foch, J. R., and Ailinger, K. G.. "Low Reynolds Number, Long Endurance Aircraft Design". AIAA Paper 92-1263, Feb. 1992.
[14] Liebeck, R. H., "Design of Subsonic Airfoils for High Lift". Journal Aircraft, vol. 15, 1978, pp. 547 - 561.
[15] Maughmer, M. D., and Somers, D. M., "Design and Experimental Results for a High-Altitude, Long-Endurance Airfoil", Journal of Aircraft, vol. 26, No. 2, 1989, pp. 148 - 153.
[16] McGhee, R. J., Walker, B. S., and Millard, B. F., "Experimental Results for the Eppler 387 Airfoil at Low Reynolds Numbers in the Langley Low-Turbulence Pressure Tunnel", NASA TM-4062, Oct. 1988.
[17] Moshe Steinbuch and Misha Shepshelovich, "Development Of high altitude long endurance airfoils", 42nd AIAA Aerospace Sciences Meeting and Exhibit 5-8 January 2004, Reno, Nevada (AIAA 2004-1052).
[18] Qiang Liu and Jie Li, "Low Reynolds Number High-Lift Airfoil Design for HALE Concept UAV", 24th Applied Aerodynamics Conference 5-8 June 2006, San Francisco, California (AIAA 2006-3462).
[19] Zhanzhong Han, Jing Wang, Xiao Ping Lan, FLUENT fluid engineering simulation examples and application (Book style), Beijing Institue Of Technology Press, CN: Beijing, 2005.
[20] Fujun Wang, Computational Fluid Dynamics - Principle and Application of CFD software, Tsinghua University Press, CN: Beijing, Sep. 2004.
[21] Zhengjuan Zhang, Hengzhang Tu, Huairong Shen, "Numerical Simulation on Wing at Low Reynolds Number on Fluent", System Simulation Technology & Application,vol.9, Aug, 2007, pp. 105-107.
[22] Peiqing Liu, Air propeller theory and its application, Beihang University Press, CN: Beijing, 2006.
[23] Baoliu Zhu, UAV aerodynamics, Beihang University Press, CN: Beijing, 2006.
[24] Yuxin Qiu, Yahong Chen, Changjia Xu, "A brief discussion of high-altitude long-endurance unmanned aerial vehicle aerodynamic research", vol. 18, Sep. 2004, pp.1-5.